

17. R. W. Ruhwandl, and E. M. Terentjev, "Long-range forces and aggregation of colloidal particles in a nematic liquid crystal," *Phys. Rev. E Stat. Phys. Plasmas Fluids Relat. Interdiscip. Topics* **55**(3), 2958–2961 (1997).
18. F. S. Y. Yeung, Y. L. J. Ho, Y. W. Li, and H. S. Kwok, "Liquid crystal alignment layer with controllable anchoring energies," *J. Display Tech* **4**(1), 24–27 (2008).
19. S. Y. Park, and D. Stroud, "Surface-enhanced plasmon plitting in a liquid crystal-coated gold nanoparticle," *Phys. Rev. Lett.* **94**(21), ,(4

under the polarizing microscope using the planar aligned cells. Uniform regions with planar alignment of smectic A liquid crystal were obtained. The optical textures as observed under the polarizing microscope were very similar to that obtained with pure 8CB when the concentration of GNPs was low as shown in Fig. 1a. However with a relatively large volume fraction ($\phi \sim 0.5$) of the GNPs, the texture exhibited an intense green color but with the focal conic like features of the smectic A phase, remaining intact as shown in Fig. 1b.



Fig. 1. Focal conic texture observed in the smectic A phase of the LC-GNP dispersions viewed between crossed polarizers, (a) $\phi = 0.21$ and (b) $\phi = 0.54$.

Optical absorption spectra were then recorded using the planar aligned cells. The spectra show that there is a progressive shift of λ_{\max}^{SPR} to longer wavelengths with increasing volume fraction of the GNPs. For the purpose of illustration we have shown in Fig. 2 the spectra for dispersions with $\phi = 0.21$ and $\phi = 0.54$ of GNPs in comparison to the spectrum obtained with the GNPs suspended in ethyl alcohol.

When the concentration of the GNPs is small the absorbance is also low leading to a marked difference in the peak absorbances for samples with $\phi = 0.21$ and $\phi = 0.54$. Though there should be a slight change in λ_{\max}^{SPR} due to the change in the host dielectric medium from

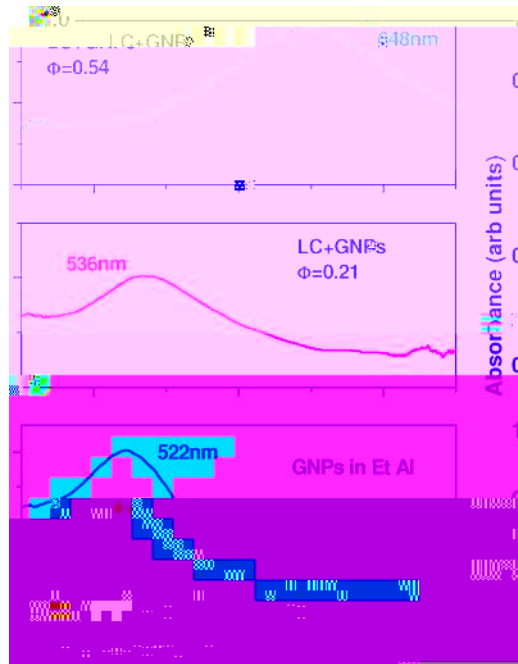
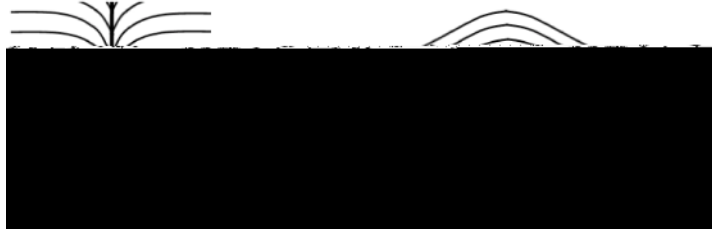


Fig. 2. Optical absorption spectra obtained with GNPs suspended in ethyl alcohol before addition of the liquid crystal and LC-GNP dispersions with $\phi = 0.21$ and $\phi = 0.54$.

We have performed absorption measurements on planar aligned samples with a light beam polarized along ($P=0^\circ$), and perpendicular ($P=90^\circ$) to the average orientation of the *director* in the bulk of the sample. The two orientations of the



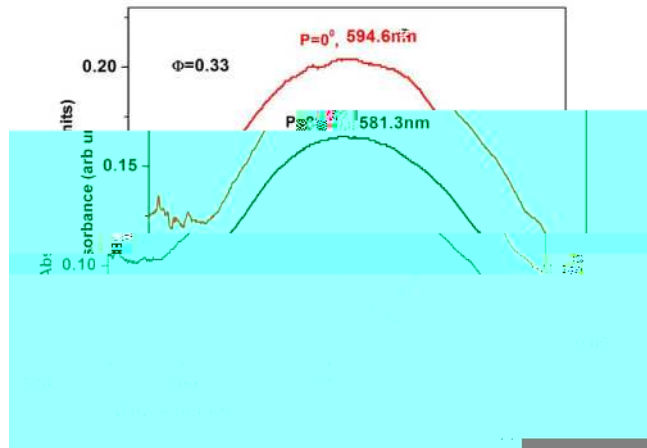


Fig. 5. Optical spectra obtained after the sample has been aligned under a magnetic field.



Fig. 6. Dependence of resonance wavelength on particle size ranging from $r=20$ to 150nm from Mie scattering calculations for refractive indexes (a) $n = 1.5$ and (b) $n = 1.7$.

In order to confirm the absence of agglomeration and also probe the distribution of the nanoparticles in the LC+GNPs samples we have used atomic force microscopy [9]. Inclusions immersed in smectic liquid crystals deform the layers resulting in a displacement of the layers along the layer normal [22–25]. When the LC-GNP dispersions are obtained in the form of thin (<100nm) films on Si substrates the nanoparticles give rise to such layer deformations resulting in raised hump like regions [9], with each hump corresponding to an individual nanoparticle, as shown in Fig. 7. The AFM images show that there is no severe agglomeration of the particles and they remain stabilized and well dispersed in the smectic A phase. The nanoparticles appear to be stabilized by repulsive interactions between particles within the same layer and limited mobility across the layers forming stable dispersions in the SmA phase [9].



Fig. 7. AFM image of the hump like regions that correspond to layer deformations induced by the nanoparticles for a sample with $\phi = 0.54$.

The Maxwell Garnet effective medium theory can be used to characterize an inhomogeneous medium by treating the material as a homogeneous substance with an effective dielectric permittivity and effective magnetic permeability. These quantities depend on the properties of the constituents, as well as on their volume fractions and sizes. Following the extended Maxwell Garnett effective medium theory, we first calculated the polarizability of individual GNP using the Mie theory and then applied the Maxwell Garnett mixing rule to calculate the complex effective index for the composite structure [10]. From the imaginary part of the n_{eff} we have calculated the absorption coefficient α for the composite structure [10].

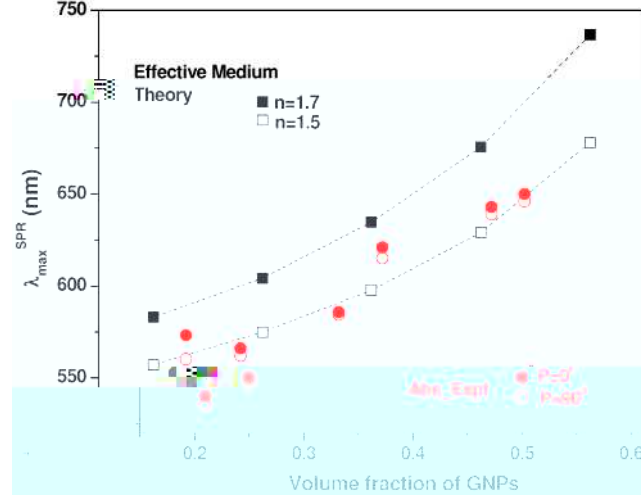


Fig. 8. Comparison of the surface plasmon resonance wavelength for different volume fraction of GNPs from effective medium calculations (dotted line drawn as guide to the eye) and from experimental absorption spectra obtained with polarizer $P=0^\circ$ and $P=90^\circ$.

Due to reasons mentioned earlier the shift in λ_{\max}^{SPR} corresponding to n_e ($P=0^\circ$) and n_o ($P=90^\circ$) is not as pronounced in the experimental data as seen in the simulations. We note that the achieved GNP volume fraction is very high in this composite. It is generally very difficult to obtain well-dispersed GNPs at high concentrations because of the large van der Waals attraction between GNPs. A recent study on GNP dispersion in organic solvents achieved volume fractions of the order of 10^{-3} [5]. In our smectic LC-GNP composite, however, the interaction between GNPs and the surrounding liquid crystal layered structure appears to prevent aggregation of GNPs even at rather high volume fractions [9]. This makes the smectic-GNP composite a highly promising material platform for novel metamaterial structures.

4. Conclusion

In conclusion, we have demonstrated the effect of an anisotropic medium on the surface plasmon resonance of the GNPs in LC-GNP dispersions. We have shown that the optical properties can be tuned by increasing the volume fraction of the GNPs. The observed dependence of the surface plasmon resonance wavelength on volume fraction of GNPs is in agreement with the effective medium theory. The realization of uniform dispersion of GNPs with high volume fraction enables the production of nanoparticle-based metamaterials, which provide an excellent alternative to nanolithographically fabricated metamaterials. While nanolithography tends to be slow and expensive, nanoparticle-based metamaterial can be fabricated by fast and cost-effective self-assembly methods. It is also straightforward to produce 3D metamaterial structures with nanoparticle dispersions, in contrast to the inherently 2D nature of lithographically fabricated structures. Extending our study to obtain stable dispersions of gold nanoparticles in ferroelectric smectic liquid crystals possessing inherent switching properties could enable tunable metamaterial architecture leading to interesting applications. Furthermore, the use of liquid crystal matrix automatically provides the possibility of dynamically tuning the metamaterial properties by external electric or optical

